Journal of Thermal Analysis and Calorimetry (2022) 147:297–313
https://doi.org/10.1007/s10973-020-10367-w

Multifunctional polyurethane foams with thermal energy storage/release capability

Francesco Galvagnini[1] · Andrea Dorigato[1] · Francesco Valentini[1] · Vincenzo Fiore[2] · Maria La Gennusa[2] · Alessandro Pegoretti[1]

Received: 16 April 2020 / Accepted: 15 October 2020 / Published online: 3 November 2020

Abstract

In this work, polyurethane (PU) insulating panels containing different amounts of a microencapsulated paraffin with a nominal melting temperature of 24 °C, used as phase change material (PCM), were produced. The resulting panels behaved as multifunctional materials able to thermally insulate and simultaneously storing/releasing thermal energy near room temperature. The panels were characterized from a microstructural, thermal and mechanical point of view. Viscosity measurements highlighted an increase in the viscosity values of the PU liquid precursors due to the addition of the capsules, and this could lead to some difficulties during the production stages, especially in the mixing and foaming phases. From optical microscopy micrographs and density measurements, it was observed that the introduction of paraffin tended to destroy the cellular structure of PU foams, and for PCM contents above 30 mass/% the foams were characterized by an open-cell morphology. SEM observations showed that PCM was preferentially distributed in the cell walls intersection, and a rather limited interfacial adhesion between capsules and PU could be detected. Thermogravimetric analysis evidenced that the introduction of the PCM tended to increase the degradation resistance of the foams, while from differential scanning calorimetry tests it was possible to conclude that PCM addition was able to impart good thermal energy storage properties to the foams, with specific melting enthalpy values of 70 J g^{-1} for a microcapsules concentration of 50 mass/%. As expected, thermal conductivity (λ) of the foams increased with PCM amount, but this enhancement was not directly related to the higher λ of the PCM itself, but rather than to the cell opening effect promoted by the PCM introduction. The microcapsules addition progressively increased the stiffness of the foams, reducing the failure properties both under quasi-static and impact conditions. Moreover, the mechanical properties were strongly affected by the testing temperature (i.e. the physical state of the wax contained in the microcapsules).

Keywords Polyurethane · Foams · Thermal energy storage · Thermal properties · Mechanical properties

Abbreviations

μ	Viscosity (cP)
$\dot{\gamma}$	Shear rate (s^{-1})
λ	Thermal conductivity (W m^{-1} K^{-1})
λ_{theo}	Theoretical thermal conductivity of the final product PU/PCM (W m^{-1} K^{-1})
λ_{PU}	Thermal conductivity of PU (W m^{-1} K^{-1})
λ_{PCM}	Thermal conductivity of PCM (W m^{-1} K^{-1})
ϕ_{PU}	Volume fraction of PU (%)
ϕ_{PCM}	Volume fraction of PCM (%)
ϕ_{CP}	Volume fraction of close pores (%)
ϕ_{OP}	Volume fraction of open pores (%)
ϕ_{Ptot}	Volume fraction of the total porosity (%)
ϕ_{CW}	Volume fraction of the cell wall (%)
T_{onset}	Temperature associated to a mass loss of 5% (°C)
T_{max1}	Temperature associated to the maximum degradation rate of PU (°C)
T_{max2}	Temperature associated to the maximum degradation rate of PCM (°C)
m_{700}	Residual mass at 700 °C (mass/%)

✉ Francesco Galvagnini
francesco.galvagnini@unitn.it

✉ Alessandro Pegoretti
alessandro.pegoretti@unitn.it

[1] Department of Industrial Engineering and INSTM Research Unit, University of Trento, Via Sommarive 9, 38123 Trento, Italy

[2] Department of Engineering, University of Palermo, Viale delle Scienze, 90128 Palermo, Italy

T_{m1}	Melting temperature measured on the first DSC scan (°C)
T_{m2}	Melting temperature measured on the second DSC scan (°C)
T_c	Temperature of crystallization (°C)
ΔH_{m1}	Specific enthalpy of fusion on the first DSC scan (J g^{-1})
ΔH_{m2}	Specific enthalpy of fusion on the second DSC scan (J g^{-1})
ΔH_c	Specific enthalpy of crystallization (J g^{-1})
$\Delta H_{m1,Rel}$	Relative enthalpy of fusion on the first DSC scan (%)
$\Delta H_{m2,Rel}$	Relative enthalpy of fusion on the second DSC scan (%)
$\Delta H_{c,Rel}$	Relative enthalpy of crystallization (%)
$t_{45°C}$	Time needed to reach 45 °C starting from 15 °C (min:s)
E	Flexural modulus of elasticity (MPa0
R	Flexural strength (MPa)
ε_{fb}	Strain at break (mm/mm)
F_m	Maximum force reached under impact test (N)
a_{cN}	Impact strength (kJ m^{-2})
E_t	Tensile elastic modulus (MPa)
σ_y	Tensile yield point (MPa)
RS	Reduced compressive strength (MPa cm^3 g^{-1})
RE_c	Reduced compressive modulus (MPa cm^3 g^{-1}

Introduction

Nowadays the energy consumption in the construction sector in the European Union covers the 41% of the total energy demand, and it is responsible for the 38% of the greenhouse gases emissions. The buildings energy consumption can be divided into 50–60% for heating, 10–25% for domestic hot water production, 3–10% for cooling and lighting systems [1]. Energy demand in building sector is expected to increase of about 50% in 2050, and the consumption related to cooling plants will triple between 2020 and 2050 [2]. It is therefore clear that this issue will play an important role for the future environmental impact and, for this reason, a massive energy consumption reduction must be achieved in the next decades [3]. For these reasons, it is essential to increase the efficiency of the buildings by using more efficient materials and technologies [1–4]. A passive way to reduce the energy consumption in buildings is the insulation of their envelope. Thermal insulating panels are a class of materials specifically designed to answer to this need. Generally speaking, insulating materials possess low thermal conductivity ($\lambda < 0.1$ W m^{-1} K^{-1}) compared with common buildings materials, like concrete and clay. They can be produced by renewable and non-renewable resources, and they can be recyclable or not. The choice of a thermal insulating material for a certain application and in a specific climatic zone does not depend only on the thermal conductivity values, but it should be performed considering an holistic approach, taking into account other important factors such as sound insulation properties, resistance to fire, water vapor permeability, impact on the environment and on human health [5–14].

Polyurethanes (PUs) represent a widespread class of materials, characterized by a great variety of properties and formulations. Polyurethanes find wide application in many industries, like shipbuilding, sports and footwear, building and automotive sector [15, 16]. Depending on their chemical composition, PUs can be thermoplastic or thermosetting, and they are constituted by urethane linkages produced by reacting diisocyanates with polyols in presence of catalysts. Polyol is usually a polyether or polyester, and it is constituted by low molecular weight polymers with hydroxyl end groups. Isocyanates can be aromatic or aliphatic precursors, with bifunctional or polyfunctional nature. From a commercial point of view, the most widely diffused isocyanates are toluene diisocyanate (TDI) and diisocyanato-diphenylmethylene (MDI). The chemical nature as well as the functionality, i.e. the number of reacting groups per molecule of reagents, should be chosen according to the intended application [17]. Additives are generally used to promote expansion (i.e. foaming agents) or to tailor material properties, like flame-retardant agents or the plasticizers. Foaming occurs when a small amount of blowing agent and water is added during polymerization process. Water reacts with isocyanate groups giving carbamic acids, which spontaneously release CO_2, generating thus foam bubbles [18, 19]. It is also possible to perform a physical blowing process, in which a liquid with a low boiling point, for example pentane, is mixed into the polyol. The reaction is exothermic and so, as it proceeds, the mixture warms up and the pentane vaporizes [19]. In residential buildings, polyurethanes can be applied to produce insulating panels, or they can be expanded on site. The resulting materials are characterized by thermal conductivity values from 0.022 to 0.040 W m^{-1} K^{-1}, density between 15 and 45 kg m^{-3}, and specific heat from 1.30 to 1.45 kJ kg^{-1} K^{-1}. Thermal conductivity generally decreases when the cell size decreases. For as concerns recycling and combustion issues, there are the same problems reported for expanded polystyrene (EPS), even if flame-retardant PUs have been extensively investigated in the last years [5].

Thermal energy storage (TES) technology is based on the accumulation of the thermal energy through a storage medium, in order to use it in a second time [20–22]. In residential buildings, TES systems could be utilized both for cooling and heating application, as they can allow a better thermal management of the indoor temperature, reducing thus daily temperature peaks and the overall energy consumption. To reach this goal, TES materials can be directly added into insulating panels or stocked

into special containers that permit heat exchange within the surrounding environment [3, 20–23]. TES materials can be divided into two groups, sensible heat storage (SHS) materials and latent heat storage (LHS) materials [4]. SHS materials exploit their heat capacity to store thermal energy, like in the case of bricks, cement, wooden beams, etc. On the other hand, the working principle of LHS materials is based on the latent heat involved in phase transformations. An important class of LHS materials are the phase change materials (PCMs), that can have organic, inorganic and eutectic nature [24–27]. PCMs are materials that absorb/release thermal energy during phase transitions in a specific temperature interval. Depending on the intended application, several types of PCM are available on the market. For indoor temperature management purposes, organic PCMs like paraffins are probably the best candidate [28–30], because their phase change temperature covers the typical indoor/outdoor temperature range. In order to avoid the problem of the PCM leakage at the molten state, PCMs can be encapsulated into organic or inorganic shells [29, 31–38].

Also building materials can be considered an interesting subject for TES applications. In fact, the use of TES materials, in combination with insulating materials, is one of the most effective way to increase the efficiency of buildings. Among materials used in buildings, concrete is one of the most used, especially for as concerns the foundations and the bearing structures. For this reason, it was one of the first materials considered in combination with TES systems [39, 40]. Ling et al. have shown that, even if the combination of concrete and encapsulated PCM is interesting from a thermal point of view, the incorporation of PCM capsules leads to a lower fire resistance, uncertain long-term stability and lower mechanical strength [28]. Royon et al. looked at the hollow areas in a concrete floor as a possible PCMs container. By filling those cavities, they were able to retain the original mechanical properties of the structure and to impart TES capability [27]. Even if insulating material represent a small part of the building envelope, they are fundamental to increase the thermal efficiency of buildings. Therefore, polymeric insulating foams were combined with different kinds of PCMs and deeply studied to couple together insulation and thermal management capabilities [23, 41–52]. Among them, PUs/PCM systems have been probably the most widely studied [30, 53–61]. This is probably due to the fact that PU is a very versatile insulating material, widely used in key industrial fields like constructions and refrigeration. In some of these articles, liquid PCM was directly added in the PU foam formulation, and it was demonstrated that PCM introduction could impart TES capability to the resulting foams. However, some problems related to the progressive leakage of the molten PCM after repeated thermal loads (i.e. day/night cycles) were evidenced [48, 55, 59]. Because of this reason, the researchers focused their attention mainly on encapsulated PCM systems [30, 53–61].

In the literature, it is possible to find some examples of PU base materials combined with TES materials, and the most important properties of these systems are reported in Table 1 [41–43, 53–55].

In the work of Borreguero, two different PCM were used, mSP-(PS-T27) (having a melting temperature of 28.5 °C) and MicronalVR DS 5001X (having a melting temperature of 27.7 °C) both encapsulated in a PMMA shell. Both PCM were incorporated in a Alcupol R-458/diphenylmethane-4,40-diisocyanat resin system and their compression properties were tested. Borreguero measured for 18 mass/% of PCM content a reduced compression strength of 2.2 MPa $cm^3\ g^{-1}$ for the first PCM and 1.1 MPa $cm^3\ g^{-1}$ for the second [39]. Serrano got similar results (3.3 2.2 MPa $cm^3\ g^{-1}$) by using 20 mass/% of the Rubitherm® RT27 PCM encapsulated in LDPE incorporated in the R-4520/Polymeric methylene diphenyl diisocyanate resin system [41].

The flexural properties of these class of composites were studied in the works of Dorigato [42] and Fredi [43]. In the study of Dorigato, the Microtek MPCM43D PCM encapsulated in a melamine–formaldehyde shell was incorporated in the Elantech EC157/W342 epoxy resin. The samples having 20 mass/% of PCM showed an elastic modulus of 2 GPa and a flexural strength of 52 MPa [42]. The results change considerably by considering the work of Fredi where the RT44HC® PCM not encapsulated was used in the same resin. Fredi got for the same mass fraction an elastic modulus of 1.4 GPa and a flexural strength of 35 MPa. This demonstrates that encapsulated PCM allow better mechanical properties with respect to not encapsulated PCM.

The greatest part of the works present in literature investigated the TES capability and the mechanical properties of the PCM-filled foams, without a comprehensive analysis of the relation between the processability, the microstructural features and the thermo-mechanical behaviour of the produced materials. On the basis of these considerations, in the present paper the following objectives and novelty aspects can be defined.

- Different amounts of a microencapsulated paraffin, having a melting temperature of 24 °C (i.e. near room temperature conditions), were added into a rigid PU matrix to produce thermal insulating panels having thermal energy storage/release capability.
- Particular attention was devoted to the investigation of the role played by PCM on the processability and the morphology of the foams, aspects that are often neglected in the open literature.
- The morphological aspects were then correlated to the most important thermo-mechanical properties of the samples.

Table 1 List of some literature references concerning PU/PCM systems

Authors	Resin system	PCM	Shell material	T_m	ΔH_m	λ	RS	RE_c	E	R	a_{cN}	Et	σ_y
Borreguero [39]	Alcupol R-458/diphenylmethane-4,40-diisocyanat	mSP-(PS-T27)	PMMA	28.5 °C	96.7 J g^{-1}	–	At 18 mass/% of PCM 2.2 MPa cm^3 g^{-1}	At 18 mass/% of PCM 48 MPa cm^3 g^{-1}	–	–	–	–	–
		Micronal VR DS 5001X	PMMA	27.7 °C	116.2 J g^{-1}	–	At 18 mass/% of PCM 1.1 MPa cm^3 g^{-1}	At 18 mass/% of PCM 16 MPa cm^3 g^{-1}	–	–	–	–	–
Amaral [40]	Purotherm 463 RG 48/puronate 900	Micronal DS 5001X	PMMA	26 °C	97.9 J g^{-1}	0.034 W m^{-1} K^{-1}	–	–	–	–	–	–	–
Serrano [41]	R-4520/Polymeric methylene diphenyl diisocyanate	Rubitherm® RT27	LDPE and ethyl-vinyl acetate (EVA)-mSD-(LDPE-EVA-RT27)	27 °C	98.1 J g^{-1}	–	At 20 mass/% of PCM 3.3 MPa cm^3 g^{-1}	At 20 mass/% of PCM 4.2 MPa cm^3 g^{-1}	–	–	–	–	–
Dorigato [42]	Elantech EC157/W342	Microtek MPCM43D	Melamine–formaldehyde	43 °C	190–200 J g^{-1}	–	–	–	At 20 mass/% of PCM 2 GPa	At 20 mass/% of PCM 52 MPa	At 20 mass/% of PCM 1.7 kJ m^{-2}	–	–
Fredi [43]	Elantech EC157/W342	RT44HC®	Not encapsulated	44 °C	219.1 J g^{-1}	–	–	–	At 20 mass/% of paraffin 1.4 GPa	At 20 mass/% of paraffin 35 MPa	–	–	–
Fredi [44]	Polyamide 12	Microtek MPCM43D	Melamine–formaldehyde	43 °C	190–200 J g^{-1}	–	–	–	–	–	–	At 30 mass/% of PCM 1 Gpa	At 30 mass/% of PCM 25 Mpa

- In this sense, this work can be considered as a first attempt to introduce some general guidelines on the development of PU foams having both insulating and thermal management capability.

Experimental part

Materials

In this work, a rigid polyurethane foam was produced mixing a HDR R 150 polyol (density = 1.1 g cm^{-3}, viscosity at 23 °C = 1050 cP) and ISN 1 isocyanate (density = 1.23 g cm^{-3}, viscosity at 23 °C = 200 cP) at a relative mass ratio equal to 100/130. Both precursors were provided by Kairos Srl (Verona, Italy). According to the information reported in the datasheet, the mixing stage can be conducted at room temperature with a cream time of 12–16 s. A microencapsulated paraffin MPCM 24, purchased by Microtek laboratories Inc. (Dayton, USA), was utilized as phase change material. This PCM was constituted by a paraffinic core surrounded by a melamine–formaldehyde shell. The relative core/shell mass ratio was 85/15, and the mean size of the capsules was about 20 μm. The melting enthalpy of the capsules declared by the producer was 24 °C, the heat of fusion was in the range 145–155 J g^{-1}, while the density at the solid state was 0.90 g cm^{-3}. A microencapsulated PCM having melamine–formaldehyde shell was selected in this work because it was directly available on the market and the authors have a long experience on the processing and the physical properties of this system. All the materials were used as received, without any further treatment.

Samples preparation

The liquid precursors (i.e. isocyanate and polyol) and the proper amount of PCM were mixed together in a beaker for 10 s at 100 rpm. For all the formulations, a polyol/isocyanate relative ratio of 100/130 was kept constant. The resulting mixtures were then poured in an aluminium mould having dimensions of 220 × 115x40 mm^3, and let then expand in an oven at 40 °C for 20 min. In this way, neat PU foam and PU foams filled with different amounts of PCM (ranging from 10 mass/% up to 50 mass/%) were prepared. Table 2 reports the list of the prepared samples, together with the adopted nomenclature and the relative concentration of the constituents.

Experimental methodologies

Viscosity measurements of the liquid precursors with different PCM amounts were performed at 23 °C through a Brookfield Dial RVT viscometer (AMETEK Brookfield, Middleboro, USA). Due to the very short cream time, viscosity could be measured only on separated liquid polyol and isocyanate systems. For these tests, a spindle number 21 was utilized, testing liquid samples with a volume of 8 mL. Optical microscope images of the polished surfaces of the foams were taken at different magnification levels by using a Zeiss Axiophot (Carl Zeiss AG, Oberkochen, Germany) microscope. The mean cell size and the cell size distribution were evaluated on the obtained micrographs by using the software Image J®. Scanning electron microscope (SEM) images of the cryofractured surface of the foams were collected by using a Zeiss Supra 40 (Carl Zeiss AG, Oberkochen, Germany) microscope, operating at an acceleration voltage of 3 kV. Before to be observed, samples were metalized by applying a Pt–Pd conductive coating.

Table 2 List of the prepared samples

Sample	PCM (mass/%)/(vol/%)	Isocyanate-ISCN (mass/%)/(vol/%)	Polyol-POL (mass/%)/(vol/%)
PU	0.0/0.0	56.5/53.8	43.5/46.2
PU-PCM10	10.0/12.6	50.9/47.0	39.1/40.4
PU-PCM20	20.0/24.5	45.2/40.6	34.8/34.9
PU-PCM30	30.0/35.8	39.6/34.5	30.4/29.7
PU-PCM40	40.0/46.4	33.9/28.8	26.1/24.8
PU-PCM50	50.0/56.5	28.3/23.4	21.7/20.1

Density measurements on the foams were performed in order to evaluate their porosity degree. At this aim, geometrical density (ρ_{geo}) was obtained simply diving the mass of the foam for their volume. Cylindrical samples having a height of 8 mm and a diameter of 10 mm were tested. In this way, a density value that considers both the open and close pores could be obtained. Theoretical density (ρ_{theo}) refers to the material without pores, and it could be calculated through the rule of mixture, knowing the density of the capsules (0.90 g cm^{-3}) and the bulk density of the neat PU matrix (0.04 g cm^{-3}). Pycnometric density (ρ_{pic}) refers to the density determined without considering the open pores, and it was determined according to the ASTM D6226 standard by using a Micromeritics AccuPyc 1330TC (Micromeritics Instrument Corp., Norcross, USA) helium pycnometer operating at room temperature, by using a testing chamber of 1 cm^3. In this way, it was possible to determine the volume fraction of the open (φ_{OP}) and of the closed (φ_{CP}) pores along with the total porosity volume fraction (φ_{Ptot}), according to the expression reported in Eq. (1–3):

$$\phi_{OP} = 100 \cdot \left(1 - \frac{\rho_{geo}}{\rho_{pic}}\right) \quad (1)$$

$$\phi_{CP} = 100 \cdot \rho_{geo} \cdot \left(\frac{1}{\rho_{pic}} - \frac{1}{\rho_{theo}}\right) \quad (2)$$

$$\phi_{\mathrm{Ptot}} = 100 \cdot \left(1 - \frac{\rho_{\mathrm{geo}}}{\rho_{\mathrm{theo}}}\right) \quad (3)$$

The cell wall fraction (φ_{CW}) was determined according to the expression reported in Eq. (4):

$$\phi_{\mathrm{CW}} = 100 \cdot \frac{\rho_{\mathrm{geo}}}{\rho_{\mathrm{theo}}} \quad (4)$$

Thermogravimetric analysis (TGA) was carried out by using a TA Q5000 IR machine (TA Instruments, New Castle, USA), operating in the temperature range between 30 °C and 700 °C, at a heating rate of 10 °C min^{-1}, under a nitrogen flow of 10 mL min^{-1}. In this way, the onset degradation temperature (T_{onset}), corresponding to the temperature associated to a mass loss of 5%, the temperatures associated to the maximum degradation rate of PU (T_{max1}) and PCM (T_{max2}), and the residual mass/% at 700 °C (m_{700}) were determined.

Differential scanning calorimetry measurements were performed through a Mettler DSC30 machine (Mettler Toledo LLC, Columbus, USA), testing samples under a nitrogen flow of 150 mL min^{-1} in aluminium crucibles with a capacity of 40 µl. After a first heating ramp from − 50 °C up to 100 °C, samples were cooled down to − 50 °C and then heated again up to 100 °C. In this way, the melting temperature in the first and second heating scans (T_{m1}, T_{m2}), the crystallization temperature in the cooling scan (T_{c}) and the associated specific enthalpy values (ΔH_{m1}, ΔH_{m2}, ΔH_{c}) were determined. Relative enthalpy values ($\Delta H_{\mathrm{m1,rel}}$, $\Delta H_{\mathrm{m2,rel}}$, $\Delta H_{\mathrm{c,rel}}$) were computed as the ratio between specific melting/crystallization enthalpy of the samples and the specific melting/crystallization enthalpy of the neat PCM, taking into account the microcapsules weight concentration (W_{PCM}) in the foams [see Eq. (5)–(7)].

$$\Delta H_{\mathrm{m1,rel}} = \left(\frac{\Delta H_{\mathrm{m1}}}{\Delta H_{\mathrm{mPCM}} \cdot W_{\mathrm{PCM}}}\right) \cdot 100 \quad (5)$$

$$\Delta H_{\mathrm{c,rel}} = \left(\frac{\Delta H_{\mathrm{c}}}{\Delta H_{\mathrm{cPCM}} \cdot W_{\mathrm{PCM}}}\right) \cdot 100 \quad (6)$$

$$\Delta H_{\mathrm{m2,rel}} = \left(\frac{\Delta H_{\mathrm{m2}}}{\Delta H_{\mathrm{mPCM}} \cdot W_{\mathrm{PCM}}}\right) \cdot 100 \quad (7)$$

Also a thermal cyclic load analysis was performed on PU-PCM30 sample to verify the thermal stability of the embedded PCM capsules. 50 cycles were performed in the temperature range from − 40 to 50 °C at a heating and cooling rate of 10 °C min^{-1}.

Limit oxygen index (LOI) measurements were performed according to ASTM D2863 standard, by using an instrument provided by Ceast (Turin, Italy). Rectangular specimens 1 × 1 × 10 cm^3 were tested at different oxygen concentrations, and at least 15 specimens were tested for each sample.

Thermal conductivity measurements were carried out by using a Laser Comp FOX 314 heat flowmeter (TA Instruments, New Castle, USA), testing samples with dimensions 20 × 300 × 300 mm^3 in a temperature range between 10 and 20 °C. At least three specimens were tested for each composition. The obtained experimental values were compared with the theoretical ones obtained applying the rule of mixture (λ_{theo}), imposing a thermal conductivity of the PCM (λ_{PCM}) equal to 0.075 W m^{-1} K^{-1} [62] and taking into account the thermal conductivity of the neat PU foam (λ_{PU}) and the volume fraction of the constituents (φ_{PU} and φ_{PCM}), as reported in Eq. (8).

$$\lambda_{\mathrm{theo}} = \lambda_{\mathrm{PU}} \cdot \phi_{\mathrm{PU}} + \lambda_{\mathrm{PCM}} \cdot \phi_{\mathrm{PCM}} \quad (8)$$

Infrared thermography was utilized to assess the TES capability of the prepared foams. Square specimens having a width of 55 mm and a thickness of 35 mm were subjected to a heating stage in an oven from 15 °C up to 50 °C, and the surface temperature in the central part of the panel was monitored through a FLIR E60 thermal camera (FLIR Systems Inc., Wilsonville, USA), placed at a distance of 30 cm from the samples. The time required to reach a surface temperature of 45 °C ($t_{45°\mathrm{C}}$) was thus determined.

Three-point bending tests were performed by using an Instron 5969 testing machine (Instron, Turin, Italy), according to the ISO 1290–2 standard. Rectangular samples 30 mm wide and 15 mm thick were tested at a crosshead speed of 20 mm/min, imposing a gage length of 180 mm. At least five specimens were tested for each composition. In order to evaluate the influence of the physical state of the PCM on the mechanical properties of the foams, the tests were performed in a thermostatic chamber at temperatures below (0 °C) and above (40 °C) the melting point of the PCM. In this way, the flexural modulus of elasticity (E), the flexural strength (R) and the flexural strain at break ($\varepsilon_{\mathrm{fb}}$) were determined. Charpy impact tests were carried out at ambient temperature (23 °C) by using a Ceast 3549/000 impact testing machine (Instron, Turin, Italy), following the ISO 179-2 standard. These tests were performed with a hammer having a length of 0.225 m, imposing an impact speed of 1 m s^{-1} and a starting angle of 39°. Rectangular specimens having a width of 15 mm, a thickness of 6 mm and a total length of 80 mm were tested. A notch with a depth of 3 mm and a radius of 0.25 mm was produced in the middle section of the specimens. A span length of 62 mm was utilized for all the samples. At least five specimens were tested for each composition. In this way, the maximum force (F_{m}) sustained by the samples and the specific energy absorbed under impact conditions (a_{cN}) were determined.

Results and discussion

One of the most important process parameters in the production of PU foams is the viscosity of the liquid precursors, that is greatly influenced by the presence of filler and/or additives in the formulation. Therefore, the shear viscosity (μ) of the ISCN/PCM and POL/PCM systems at different microcapsules amount was investigated, and its trend as a function of the applied shear rate is reported in Fig. 1a, b. As it could be expected, the viscosity decreases with the applied shear rate, but the introduction of the PCM at elevated concentrations determines an important increase in the μ values, especially in the low shear rate region. For ISCN/PCM system, the shear viscosity at a shear rate of 5 s^{-1} increases by 17.5 times for a PCM content of 30 mass/%, while for POL/PCM formulations a 4.5-fold increase can be detected at the same shear rate with a capsule concentration of 20 mass/%. For higher PCM amounts, it was impossible to collect the shear viscosity data, because the required torque would be too high for the utilized testing equipment. These results highlight that some problems could arise during the production steps of these foams, as the experienced viscosity increase could negatively affect the homogeneity and the microstructural behaviour of the produced foams.

Considering that the thermo-mechanical properties of the foams are strictly related to their morphology, optical microscopy observations were carried out in order to investigate the cell structure of the produced materials. In Fig. 2, optical microscope images of the prepared foams at different PCM contents and at two magnification levels (16× and 500x) are collected.

From images at 16× magnification, it can be immediately noticed that the sample microstructure changes from a regular close cell morphology (PU sample) to an irregular open pore structure (PU-PCM50 sample), meaning that the progressive addition of the PCM is responsible of the so-called PCM cell opening effect. It could be thus hypothesized that the viscosity enhancement observed at elevated PCM concentrations negatively affects the homogeneization of the liquid mixture and hinders the formation of a regular close-cell structure. On the other hand, optical microscope images at higher magnification level (500x) show that PCM microcapsules are mainly located at the cell wall intersection, and thus the extension of this region in PU-PCM30 and PU-PCM50 samples is significantly higher than that detected in the neat PU foam. Analysing the obtained micrographs with the Image J® software, it is also possible to investigate the pore size distribution, as reported in Fig. 3.

In Table 3, the most important results of this analysis are expressed in terms of mean pore size and the Full Width at Half Maximum (FWHM) of the distribution. Considering standard deviation values associated to these measurements, it is evident that the mean pore size is not strongly affected by PCM addition within the PU matrix, but the FWHM values are strongly increased with the capsules amount. For instance, neat PU foam presents a FWHM value of about 150 μm, while for PU-PCM50 sample a FWHM of about 500 μm can be registered. Once again, this means that PCM addition somehow hinders the formation of a regular cell structure, and this feature will probably negatively affect the thermo-mechanical behaviour of the produced foams.

Another important microstructural feature that could strongly affect the mechanical behaviour of the resulting foams is related to the surface adhesion between the PU matrix and the capsules. Therefore, SEM images of the cryo-fractured surface of the prepared foams were collected, and the micrographs taken at a magnification level of 5000× are reported in Fig. 4.

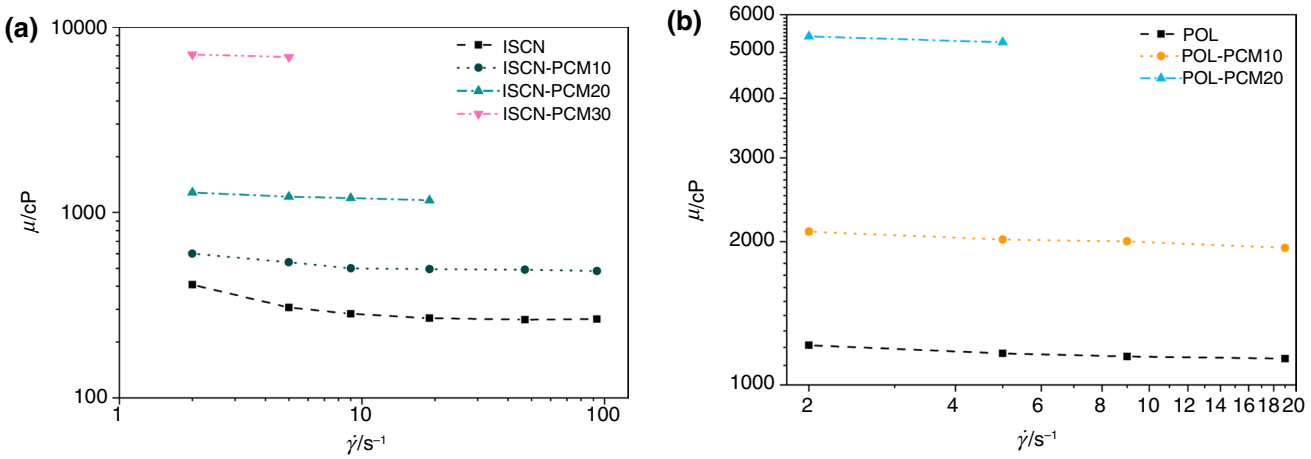

Fig. 1 **a** Viscosity-shear rate plots of ISCN-PCMx (x = 10–30 mass/%) and **b** POL-PCMx (x = 10–20 mass/%) liquid mixtures

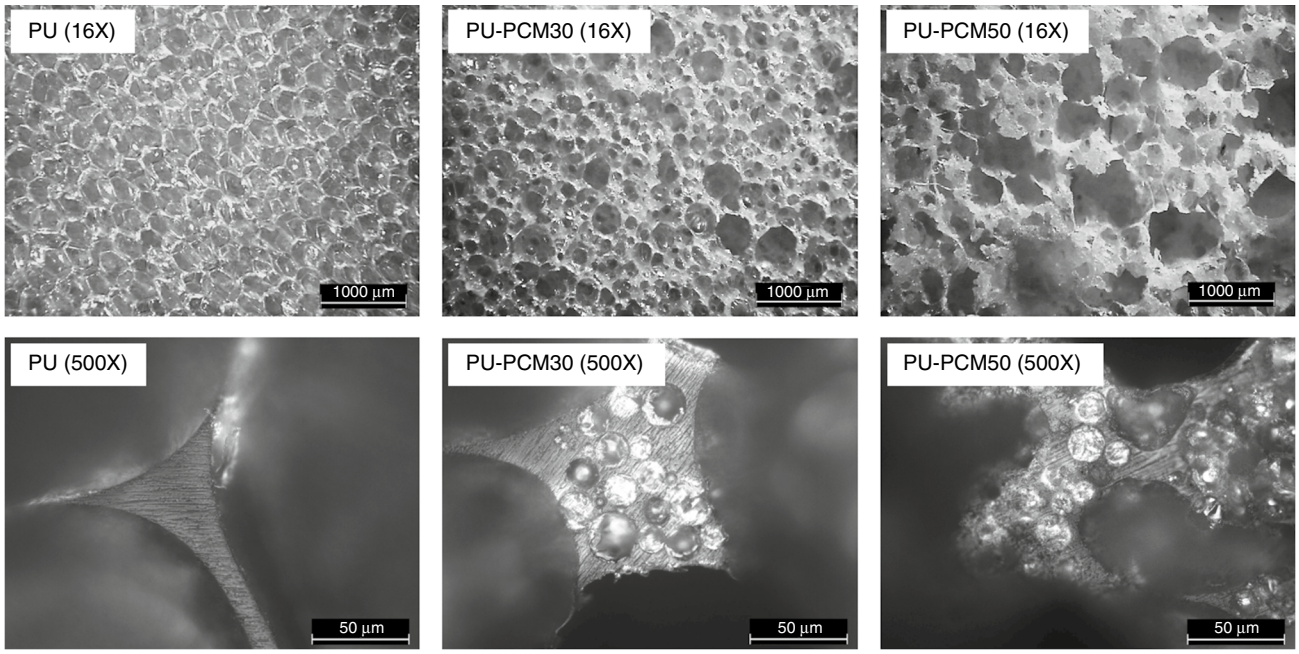

Fig. 2 Optical microscopy images of PU, PU-PCM30 and PU-PCM50 foams at different magnification levels

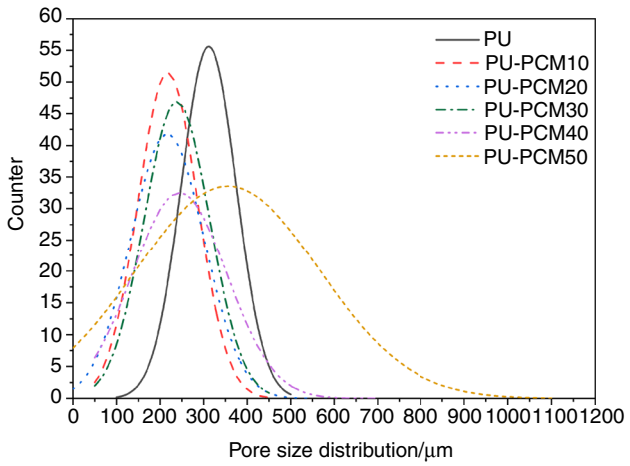

Fig. 3 Pore size distribution of the prepared foams

Table 3 Pore size distribution of the prepared foams

Sample	Mean pore size/µm	FWHM/µm
PU	311.7 ± 63.2	148.6
PU-PCM10	217.6 ± 68.3	160.6
PU-PCM20	216.8 ± 84.1	198.2
PU-PCM30	238.6 ± 74.9	176.2
PU-PCM40	244.8 ± 108.1	254.4
PU-PCM50	355.5 ± 208.4	493.3

FWHM Full Width at Half Maximum

These images confirm that the capsules are mainly located at the cell wall intersection, by they also highlight a weak interfacial adhesion between the PU matrix and the microcapsules organic shell. From these micrographs, it is evident the presence of a partial debonding at the interface, especially if the PU-PCM30 foam is observed. It must be also considered that the chemical compatibility between the PU matrix and the melamine–formaldehyde shell of the capsules is probably rather low, and this feature will probably negatively affect the failure properties of the prepared materials. Further efforts will be made in the future to improve the chemical compatibility between the PCM and the PU, trying to introduce a surface functionalization on the microcapsules shell.

In order to have further insights on the cell morphology of the foams, density measurements were performed by using different techniques, and the trends of the open (φ_{OP}), close (φ_{CP}) and total porosity (φ_{Ptot}) as a function of the PCM amount is reported in Fig. 5.

As it could be expected observing optical microscope and SEM micrographs, the introduction of the PCM within the PU foams determines a noticeable increase in the open pores, at the expenses of the close porosity. If in the neat PU sample a φ_{OP} value of 36% can be registered, for PCM contents higher than 20 mass/% φ_{OP} is almost 90%. This means that the microstructure of the foams at elevated capsules amount is mainly characterized by an open-pore morphology. It is clear that this change in pore structure will play a key role on the mechanical behaviour and on the thermal conductivity of the resulting foams. In fact, it

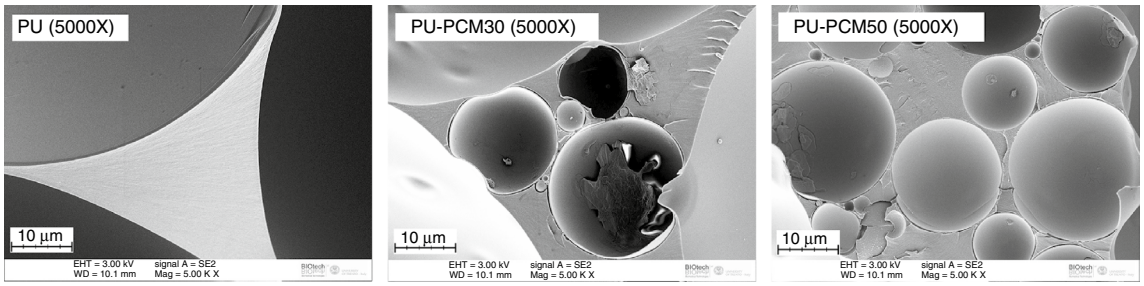

Fig. 4 Scanning electron microscope images of PU, PU-PCM30 and PU-PCM50 foams (magnification 5000x)

is well known that close cell foams have in general higher

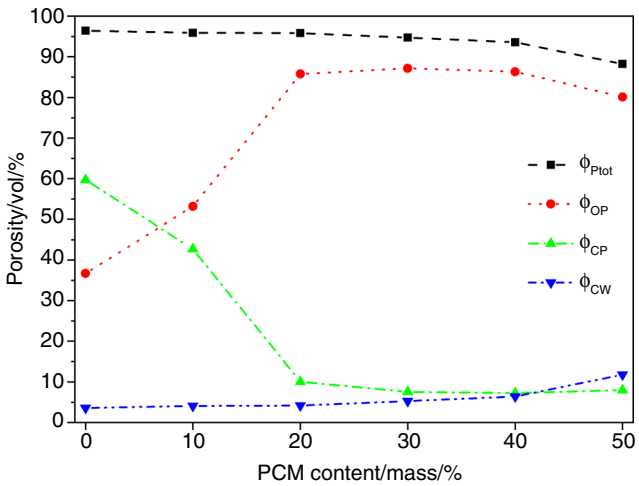

Fig. 5 Evaluation of the porosity degree of the prepared foams

mechanical resistance with respect to insulating panels with open pores. On the other hand, the presence of open pores within the materials allows the inner air to move within the pores, with a consequent increase in the thermal conductivity values. On the contrary, sound insulation properties are improved if an open-cell structure is formed [5]. It is therefore clear that the evaluation of the effect of the PCM addition in these foams is strictly connected to their intended application. Interestingly, both the total porosity (φ_{Ptot}) and the cell wall concentration (φ_{CW}) are not strongly influenced by the PCM addition, and only a slight decrease in the pore concentration (from 96% up to 90%) can be detected for a PCM amount of 50 mass/%.

It is also clear that the microstructural features of the prepared foams could strongly influence their thermal degradation behaviour. Therefore, TGA measurements were performed. In Fig. 6a, b the trends of the residual mass and of the derivative of the mass loss with the testing temperature are represented, while in Table 4 the most important results are collected.

It is interesting to notice that the PCM microcapsules have a superior thermal degradation stability with respect to the foams, and the degradation takes places in a single step located at around 400 °C. On the other hand, neat PU foams manifest a main degradation peak at about 330 °C. As a consequence, the TG curves of the PU/PCM foams are characterized by two degradation steps, corresponding to the degradation of the PU matrix (T_{max1}) and of the PCM capsules (T_{max2}). The position of these peaks does not seem to be correlated to the PCM amount within the foams. It is important to observe that the introduction of the microcapsules is responsible of an interesting improvement in the thermal stability of the foams, with a progressive increase in the T_{onset} values. For the PU-PCM30 sample, a T_{onset} increase of more than 20 °C can be observed with respect to the neat PU foam. Once again, this feature could be interesting for those applications in which insulating materials with improved thermal degradation resistance are required. Considering the mass residue at 700 °C, it can be noticed that the residue of the neat PCM is about 1%, while for neat PU foam a m_{700} value of 22% can be registered. Moreover, m_{700} values systematically decrease with the PCM content. This is probably related to the crosslinked nature of the PU foams and to the formation of a carbonaceous char on the surface of the samples, that hinders the further degradation of the samples core at elevated temperatures.

In order to evaluate the thermal energy storage capability of the prepared foams, DSC tests were performed. In Fig. 7 DSC, curves of the samples collected in the first heating stage are reported, while the trend of the most important thermal properties is numerically shown in Table 5.

From the DSC curves, it is evident the presence of the endothermic peak associated to the melting of the microcapsules, ad its position (i.e. T_{m1}) does not seem to depend to the PCM concentration. On the other hand, a progressive increase in the specific melting enthalpy with the paraffin amount can be detected. For instance, a ΔH_{m1} value of 70 J g^{-1} can be registered for the PU-PCM50 sample. This means that TES capability of the foams increases with the PCM content. Also the position of the crystallization

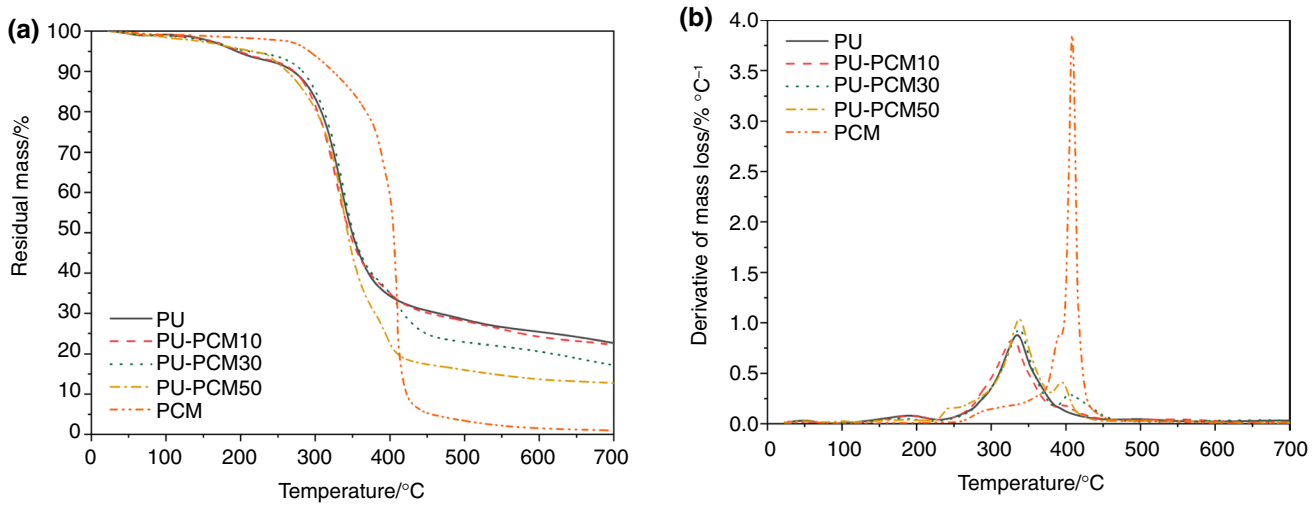

Fig. 6 TGA results of the prepared samples. **a** TGA curves and **b** derivative mass loss curves

Table 4 Results of TGA tests on the prepared foams

Sample	T_{onset}/°C	T_{max1}/°C	T_{max2}/°C	m_{700}/ mass/%
PU	194.7	334.7	–	22.6
PU-PCM10	198.5	329.1	397.4	22.2
PU-PCM30	211.1	337.7	405.6	17.2
PU-PCM50	216.5	337.6	394.4	12.8
PCM	292.2	–	408.5	1.0

T_{onset} temperature associated to a mass loss of 5 mass/%. T_{max1} temperature corresponding to the first maximum of mass loss derivative curves, related to PU degradation. T_{max2} temperature corresponding to the second maximum of mass loss derivative curves related to PCM degradation. m_{700} residual mass at 700 °C

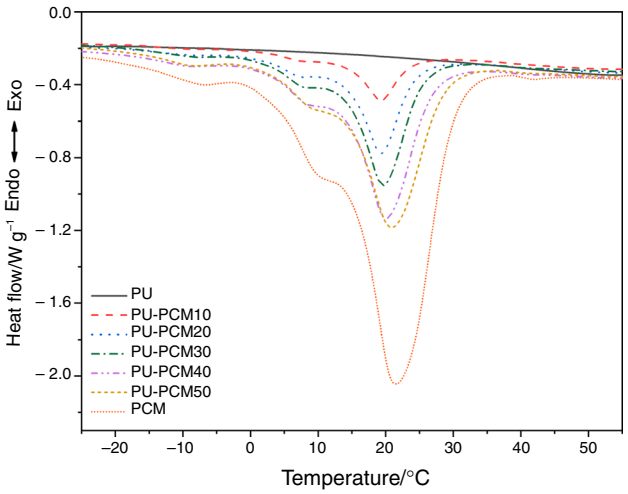

Fig. 7 DSC curves of the prepared foams (first heating stage)

temperature (T_c) and of the melting temperature in the second heating stage (T_{m2}) is not related to the PCM amount, and the specific melting enthalpy values associated to these transition are very similar to those registered in the first heating stage. It is also interesting to notice that relative melting enthalpy ($\Delta H_{m1,rel}$, $\Delta H_{m2,rel}$) and relative crystallization enthalpy ($\Delta H_{c,rel}$) values of the prepared foams are around 100% for all the investigated compositions. This means that the microcapsules are able to retain their structural integrity (and thus their TES capability) even after the processing of the foams. A similar conclusion has been already reported in our previous works in which PCM capsules have been added to a novel reactive thermoplastic resin (Elium®) [44].

In Fig. 8, a comparison between the heating curves taken at different DSC cycles for the PU-PCM30 sample is reported, while the most important results are summarized in Table 6. In the first cycle, the measured melting enthalpy was 40.5 J g^{-1}, while in the fiftieth cycle it was 41.2 J g^{-1}, and also the melting temperature does not substantially change with the application of cyclic DSC tests. From these results it is clear that there are no problems related to the PCM leakage upon repeated thermal cycles, and the microcapsules retain their integrity even after the applications of cyclic thermal loads.

In order to get further insights on the thermal degradation and on the flame behaviour of the prepared materials, Limiting Oxygen Index (LOI) measurements were performed, and the results are summarized in Table 7.

It is important to underline that the introduction of the PCM within the PU foam leads to a slight decrease in the LOI values, proportionally to the capsules content. If neat PU samples show a LOI value of 19.7 vol/%, a decrease of 2 vol/% can be registered for the PU-PCM50 sample. This result can be explained considering that PCM is constituted

Table 5 Results of DSC tests on the prepared foams

Sample	T_{m1}/°C	ΔH_{m1}/J g^{-1}	$\Delta H_{m1,rel}$/%	T_c/°C	ΔH_c/J g^{-1}	$\Delta H_{c,rel}$/%	T_{m2}/°C	ΔH_{m2}/J g^{-1}	$\Delta H_{m2,rel}$/%
PU-PCM10	19.36	12.54	93.4	11.91	14.14	100.9	19.55	13.60	101.4
PU-PCM20	19.27	26.89	100.2	11.79	26.06	93.0	19.55	27.76	103.5
PU-PCM30	19.61	40.15	99.7	11.45	41.92	99.7	19.64	39.61	98.5
PU-PCM40	20.10	53.52	99.7	11.13	59.54	106.2	20.12	54.01	100.7
PU-PCM50	20.78	70.50	105.1	9.82	70.49	100.6	20.97	71.34	106.4
PCM	21.59	134.19	–	10.69	140.14	–	21.61	134.05	–

ΔH_{m1} specific melting enthalpy (first heating scan), ΔH_c specific crystallization enthalpy (cooling scan), ΔH_{m2} specific melting enthalpy (second heating scan), T_{m1} melting temperature (first heating scan), T_c crystallization temperature (cooling scan), T_{m2} melting temperature (second heating scan), $\Delta H_{m1,rel}$ relative melting enthalpy (first heating scan), $\Delta H_{c,rel}$ relative crystallization enthalpy (cooling scan), $\Delta H_{m2,rel}$ relative melting enthalpy (second heating scan)

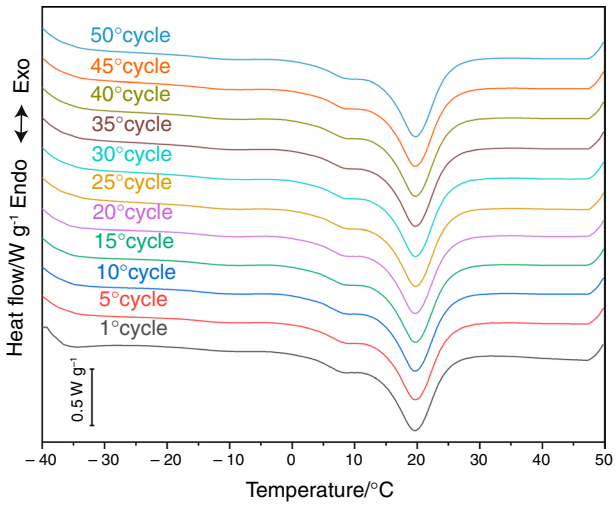

Fig. 8 DSC curves of the PU-PCM30 foam at different number of thermal cycles

Table 6 Results of the DSC tests performed on PU-PCM30 at different number of thermal cycles

Cycle	T_{m1}/°C	ΔH_m/J g^{-1}	T_c/°C	ΔH_c/J g^{-1}
1	19.60	40.51	14.29	44.29
5	19.79	41.50	14.12	43.32
10	19.92	41.81	13.96	42.53
15	19.78	41.75	13.80	42.33
20	19.62	41.27	13.97	43.14
25	19.77	41.12	13.97	42.26
30	19.60	40.32	13.98	41.70
35	19.77	41.03	14.15	41.88
40	19.77	41.46	14.14	42.06
45	19.61	41.26	13.97	41.92
50	19.77	41.19	13.89	41.34

Table 7 Limiting Oxygen Index (LOIs) values of the prepared foams

Sample	LOI (vol/% O_2)
PU	19.7 ± 0.1
PU-PCM10	18.9 ± 0.1
PU-PCM20	18.8 ± 0.2
PU-PCM30	18.6 ± 0.2
PU-PCM40	18.1 ± 0.1
PU-PCM50	17.6 ± 0.2

by a paraffinic material with a rather low molecular weight, and it is therefore clear that the flammability of the PCM is lower than that of a thermosetting matrix like PU. However, the observed LOI decrease is not dramatic, and the foams with PCM retain their applicability for the greatest part of the technological applications in which they are currently utilized.

One of the key features of thermal insulating materials is the thermal conductivity. Moreover, this physical property plays a key role also in TES applications, as it determines the thermal diffusivity through the materials and thus its heat exchange capability. Therefore, thermal conductivity measurements were performed on the prepares foams, and the resulting values collected in the temperature interval 10–20 °C ($\lambda_{10\text{-}20\ °C}$) are represented in Fig. 9.

In the same plot, also the theoretical values (λ_{theo}) determined through the rule of mixture [see Eq. (8)] are reported. As expected, the thermal conductivity increases with the PCM content, but the observed enhancement is not dramatic until a capsules amount of 30 mass/%. Due to the substantial difference between the density of the PU foam and that of the PCM, it is clear that the volume concentration of paraffin within the prepared samples is rather low, even at elevated PCM concentrations. This means that the thermal insulating properties of the foams are not heavily impaired upon microcapsules addition. On the other hand, the heat exchange capacity of the resulting foams remains rather limited, even at elevated PCM concentrations. It is interesting

to notice that experimental values follow the theoretical ones until a paraffin amount of 30 mass/%, while for higher PCM contents a substantial deviation from λ_{theo} values can be detected. This discrepancy can be explained considering the cell opening effect promoted by PCM addition in elevated concentrations. As reported in optical microscope images (Fig. 2), the regular cell structure is destroyed in PU-PCM50 sample, and an open-cell morphology can be detected. In these conditions, the entrapped air can freely move within the pores, with a consequent thermal conductivity enhancement.

In order to simulate the TES behaviour of the prepared foams under real exercise conditions, some panels were subjected to a thermal cycle from 15 °C up to 50 °C, and the trends of the surface temperature (T_{ss}) with the testing time were collected. The T_{SS} values of the foams at different PCM amounts are reported in Fig. 10, while the time required to reach a surface temperature of 45 °C ($t_{45°C}$) is shown in Table 8.

From this plot, it is immediately evident that the introduction of PCM is responsible of an important temperature shift, and the foams at elevated PCM contents show a delayed heating with respect to the neat PU. For instance, if the neat PU foam reaches a surface temperature of 45 °C after 2 min, a delay of more than 20 min can be detected with a PCM amount of 40 mass/%. This confirms the TES capability of the prepared foams at elevated PCM contents, and the possibility to use these materials for thermal management applications in the building sector.

Finally, the mechanical behaviour of the prepared foams was evaluated, and the flexural properties of the samples below (0 °C) and above (40 °C) the melting temperature of the PCM were determined. In Fig. 11a, b representative

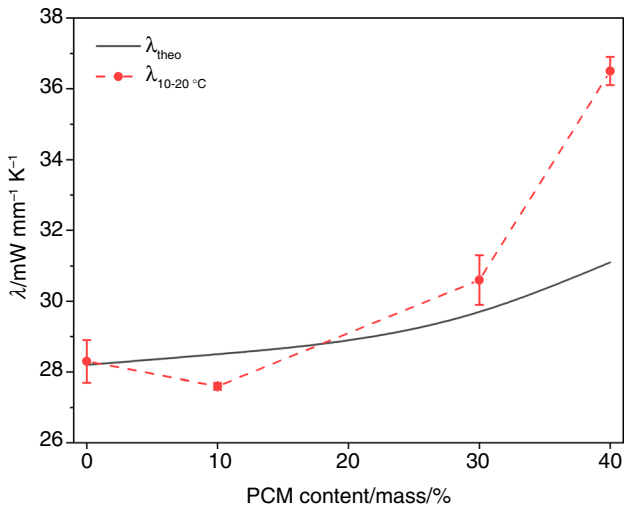

Fig. 9 Comparison between experimental and theoretical thermal conductivity values of the prepared foams

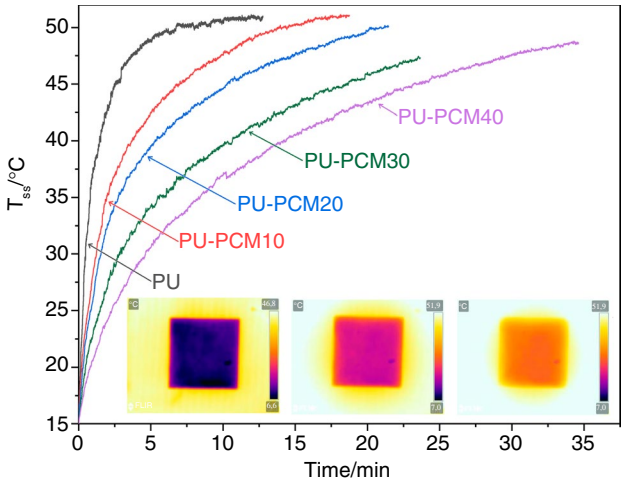

Fig. 10 Evolution of the foam's surface temperature detected by infrared thermal camera as a function of the testing time

stress–strain curves collected at 0 °C and 40 °C are, respectively, collected, while in Fig. 11c–e the trend of the flexural modulus (E), of the flexural strength (R) and of the strain at break (ε_{fb}) as a function of the PCM amount is, respectively, reported. Regardless to the testing temperature, it is clear that neat PU foam has a rather high deformation at break (some samples were not broken during the tests), while the introduction of PCM is responsible of an increase in the stiffness, associated to a substantial reduction in the strain at failure. In fact, the stiffness of the PU-PCM50 sample is about two times than that of the neat PU foam, while ε_{fb} values are considerably reduced, even at limited PCM contents. Quite interestingly, the stress at break does not seem to be heavily affected by the paraffin introduction, neither at elevated PCM amounts. The reduction in the strain at break detected in Fig. 11e can be probably related to the low interfacial adhesion between the PU matrix and the microcapsules detected in SEM micrographs (see Fig. 4) and to the aggregation of the capsules at the cell wall intersection (see Fig. 2). Also the cell opening effect promoted by PCM introduction at elevated concentrations should be taken into account. In these conditions, PCM acts as a defect

Table 8 Time required to reach a surface temperature of 45 °C of the prepared foams, from infrared thermal camera measurements

Sample	$t_{45°C}$ (min:s)
PU	2:32
PU-PCM10	7:00
PU-PCM20	10:18
PU-PCM30	18:40
PU-PCM40	23:12

$t_{45°C}$ time required to reach 45 °C, starting from 15 °C

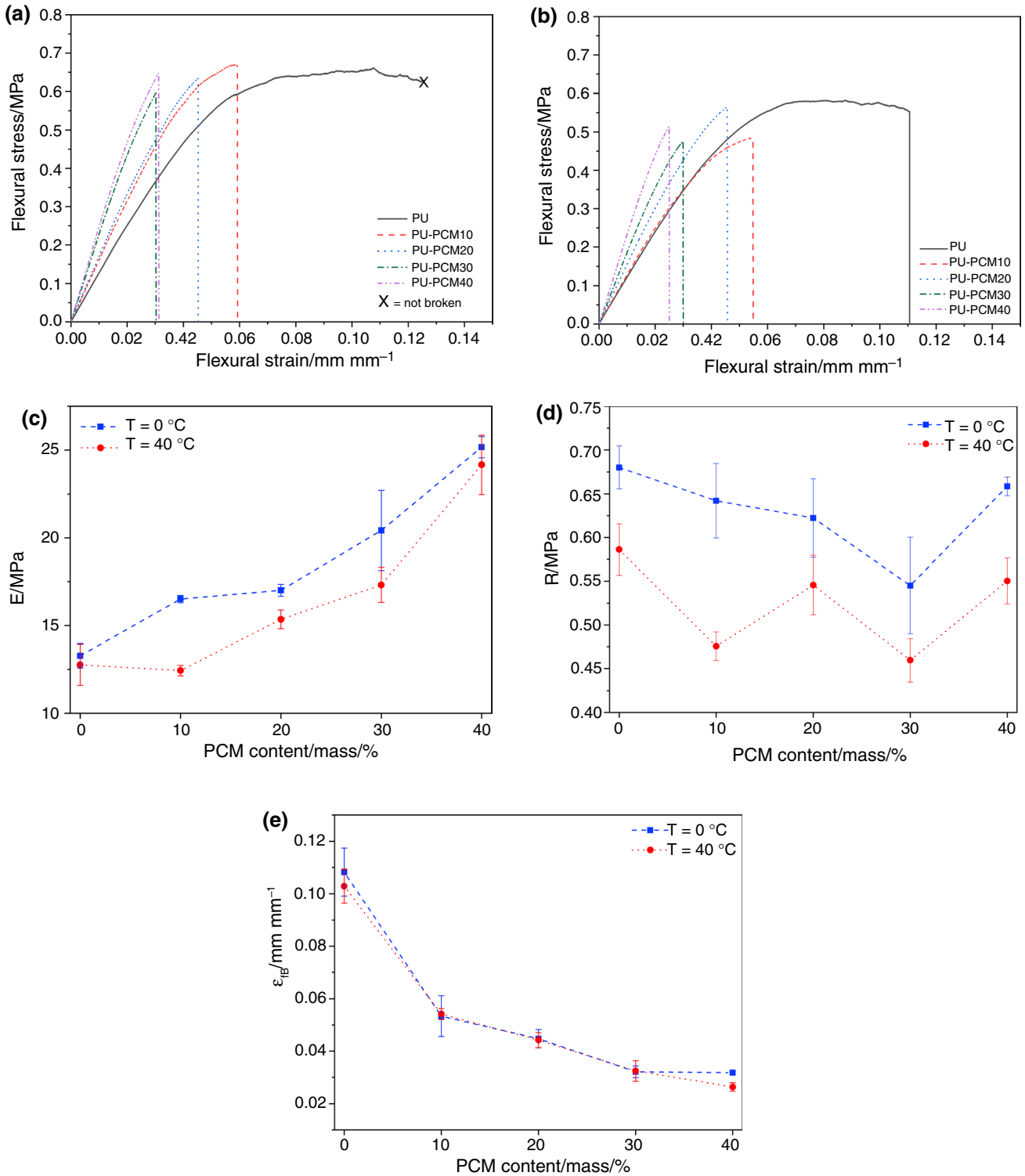

Fig. 11 Three-point bending tests on the prepared samples. **a** Stress–strain curves at 0 °C, **b** stress–strain curves at 40 °C, **c** elastic modulus, **d** flexural strength and **e** flexural strain at break as a function of the PCM amount and of the testing temperature

in the material, producing thus a strong embrittling effect. A similar trend has been also observed by our group in a TPU matrix filled with paraffin microcapsules [48, 49]. It is also important to investigate the effect of the physical state of the PCM on the mechanical properties of the resulting foams. In fact, this aspect is often neglected in the open

literature. From the plots reported in Fig. 11c, d it is possible to observe that both the stiffness and the stress at break of the foams tested at 40 °C are systematically lower than those detected at 0 °C.

However, considering the standard deviation values associated to these measurements and the obtained trends, it is difficult to assess if the observed drop above the melting temperature of the PCM is due to the decrease in the mechanical properties of the capsules at the molten state or to a drop of the mechanical performances of the PU matrix at elevated temperature. It is probable that both these aspects will affect the mechanical behaviour of the foams at 40 °C, but further efforts will be necessary to have a better comprehension of these aspects.

Also the impact properties of the prepared foams were evaluated, and in Fig. 12 representative force–time curves from Charpy impact tests are reported, while the most important numerical results in terms of maximum force (F_m) and specific impact strength (a_{cN}) are summarized in Table 9.

In accordance with quasi-static flexural tests, it is evident that the PCM introduction is responsible of an important embrittlement of the samples, even at limited microcapsules contents. For instance, PU-PCM30 sample shows a specific impact strength corresponding to one third of that of the neat PU (it was impossible to tests the samples with higher microcapsules amount, because they were too brittle). In this case, also the maximum force is heavily reduced upon PCM addition. Once again, this embrittling effect is related to the low homogeneity of the pore structure, to the aggregation of the PCM at the cell wall intersection and to the rather low interfacial adhesion between the PU matrix and the capsules. The decrease in the toughness observed both

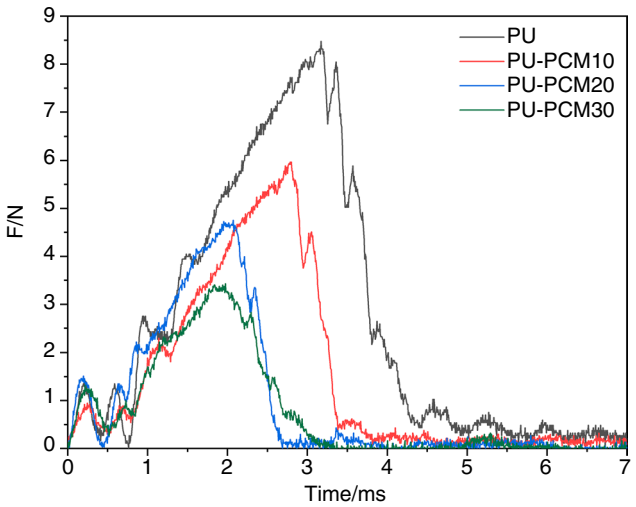

Fig. 12 Representative force–time curves from Charpy impact tests on the prepared foams

Table 9 Results of Charpy impact tests on the prepared foams

Sample	F_m/ N	a_{cN}/kJ m^{-2}
PU	7.34 ± 0.24	0.24 ± 0.03
PU-PCM10	5.92 ± 0.22	0.14 ± 0.02
PU-PCM20	4.69 ± 0.27	0.08 ± 0.01
PU-PCM30	3.78 ± 0.21	0.07 ± 0.01

F_m maximum impact force, a_{cN} Charpy notched impact strength

under quasi-static and impact conditions must be seriously taken into account considering the possible application of these materials as thermal insulating panels, and further efforts will be made in the future to improve the dispersion of the PCM within the PU matrix. Some attempts will be also made to introduce a functionalization on the surface of the capsules, in order to improve the interfacial adhesion.

Conclusions

Novel multifunctional thermal insulating panels, able to store/release thermal energy near room temperature, were prepared combining a PU foamed matrix with a microencapsulated paraffin at different concentrations. Different analyses were performed on the produced material to study its morphological, thermal and mechanical properties. According to the obtained results, some conclusions can be drawn.

- The viscosity of the liquid precursors was considerably increased upon the PCM addition, leading to some difficulties in the mixing and the foaming steps.
- Microstructural characterization and density measurements evidenced that capsules addition at elevated amounts led to the formation of an open-cell morphology, increasing also the statistical dispersion of the pore size.
- TGA tests highlighted that PCM addition was responsible of an increase in the thermal degradation resistance, while flame behaviour was slightly deteriorated upon paraffin introduction, with a limited decrease in the LOI values.
- DSC tests and infrared thermal camera images demonstrated that the presence of microcapsules within the PU foams at elevated concentrations was able to impart good TES properties to the foams.
- The experienced increase in the thermal conductivity at a PCM content of 50 mass% was directly related to the cell opening effect due to the PCM introduction.
- Regardless to the testing temperature (i.e. the physical state of the PCM), microcapsules addition within the foams was responsible of an important stiffening effect,

associated to a substantial decrease in the failure properties both under quasi-static and impact conditions.

From the results of this study, it is evident that a common insulating material such as a polyurethane rigid foam could also be endowed with thermal energy storage capability by incorporating PCM capsules in the proper amount. This feature could be helpful to reduce the thermal energy wastes, to increase the energy efficiency of the buildings and to reduce the greenhouse gases emissions in the building sector. In this study, the most promising composition was PU-PCM30 for its good compromise between mechanical and thermal properties. Considering a price of 3.40 €/kg for the PU foam and 50.00 €/kg for the microcapsules (data taken from the producers), a cost increase between 6 and 7 times can be expected for this material. According to the authors' opinion, this cost increase is still not sustainable. Nevertheless, future cost reduction in the PCM due to scale economy and the increasing interest towards thermal management issues in residential sector can be expected.

Future research activities should be focused on the production of foamed polymers having higher amount of PCM and superior mechanical properties. In this sense, the adhesion between PCM capsules and PU matrix should be enhanced to limit the interfacial debonding during the application of mechanical loads.

Author contributions Conceptualization: Francesco Galvagnini, Andrea Dorigato and Francesco Valentini. Data curation: Francesco Galvagnini, Vincenzo Fiore and Maria La Gennusa. Formal analysis: Francesco Galvagnini, Vincenzo Fiore and Maria La Gennusa. Funding acquisition: Andrea Dorigato and Alessandro Pegoretti. Investigation: Francesco Galvagnini, Andrea Dorigato and Francesco Valentini. Methodology: Francesco Galvagnini, Andrea Dorigato and Francesco Valentini. Supervision: Andrea Dorigato and Alessandro Pegoretti.

Funding This work was partially funded by University of Trento and by Provincia Autonoma di Trento through Legge 6/99, project "Compositi elastomerici a transizione di fase [E-PCM] prat. n. 23-16".

Availability of data and material This manuscript has no associated data or the data will not be deposited

Code availability This manuscript has no associated code.

Compliance with ethical standards

Conflicts of interest The authors declare that they have no known competing financial interests or personal relationships that could have appeared to influence the work reported in this paper.

References

1. Sarbu I, Sebarchievici C. Introduction. Sol Heat Cool. Syst. 2017. p. 1–11.
2. Pacheco-Torgal F. Introduction to Cost-Effective Energy-Efficient Building Retrofitting. In: Pacheco-Torgal F, Granqvist C-G, Jelle BP, Vanoli GP, Bianco N, Kurnitski J, editors. Cost-Effective Energy-Efficient Building Retrofitting. Woodhead Publishing; 2017. pp. 1–20.
3. Stritih U, Tyagi VV, Stropnik R, Paksoy H, Haghighat F, Joybari MM. Integration of passive PCM technologies for net-zero energy buildings. Sustain Cities Soc. 2018;41:286–95. https://doi.org/10.1016/j.scs.2018.04.036.
4. Zadeh FM. Integration of phase change materials in commercial buildings for thermal regulation and energy efficiency [Master Thesis]: University of Arizona; 2015.
5. Schiavoni S, D'Alessandro F, Bianchi F, Asdrubali F. Insulation materials for the building sector: A review and comparative analysis. Renew Sustain Energy Rev. 2016;62:988–1011. https://doi.org/10.1016/j.rser.2016.05.045.
6. Ricciu R, Besalduch LA, Galatioto A, Ciulla G. Thermal characterization of insulating materials. Renew Sustain Energy Rev. 2018;82:1765–73. https://doi.org/10.1016/j.rser.2017.06.057.
7. Pargana N, Pinheiro MD, Silvestre JD, De Brito J. Comparative environmental life cycle assessment of thermal insulation materials of buildings. Energy Build. 2014;82:466–81.
8. Kylili A, Fokaides PA. Methodologies for Selection of Thermal Insulation Materials for Cost-Effective, Sustainable, and Energy-Efficient Retrofitting. In: Pacheco-Torgal F, Granqvist C-G, Jelle BP, Vanoli GP, Bianco N, Kurnitski J, editors. Cost-Effective Energy-Efficient Building Retrofitting. Woodhead Publishing; 2017. p. 23–55.
9. Kumar A, Suman BM. Experimental evaluation of insulation materials for walls and roofs and their impact on indoor thermal comfort under composite climate. Build Environ. 2013;59:635–43. https://doi.org/10.1016/j.buildenv.2012.09.023.
10. Jelle BP. Traditional, state-of-the-art and future thermal building insulation materials and solutions—Properties, requirements and possibilities. Energy Build. 2011;43(10):2549–63. https://doi.org/10.1016/j.enbuild.2011.05.015.
11. Hall MR. Part II, Materials for energy efficiency and thermal comfortin buildings. In: Hall MR, editor. Materials for Energy Efficiency and Thermal Comfort in Buildings. Woodhead Publishing; 2010. p. 173–502.
12. D'Alessandro F, Baldinelli G, Bianchi F, Sambuco S, Rufini A. Experimental assessment of the water content influence on thermo-acoustic performance of building insulation materials. Constr Build Mater. 2018;158:264–74. https://doi.org/10.1016/j.conbuildmat.2017.10.028.
13. Berardi U, Naldi M. The impact of the temperature dependent thermal conductivity of insulating materials on the effective building envelope performance. Energy Build. 2017;144:262–75. https://doi.org/10.1016/j.enbuild.2017.03.052.
14. Abdou AA, Budaiwi IM. Comparison of thermal conductivity measurements of building insulation materials under various operating temperatures. J Build Phys. 2016;29(2):171–84. https://doi.org/10.1177/1744259105056291.
15. Pegoretti A, Dorigato A, Brugnara M, Penati A. Contact angle measurements as a tool to investigate the filler–matrix interactions in polyurethane–clay nanocomposites from blocked prepolymer. Eur Polym J. 2008;44(6):1662–72. https://doi.org/10.1016/j.eurpolymj.2008.04.011.
16. Dorigato A, Pegoretti A, Penati A. Effect of the polymer—filler interaction on the thermo-mechanical response of polyurethane-clay nanocomposites from blocked prepolymer. J Reinf Plast

Compos. 2011;30(4):325–35. https://doi.org/10.1177/0731684410396599.
17. Woods G. An introduction to polyurethanes. The ICI Polyurethanes Book. John Willey and Sons; 1990. p. 1–6.
18. Woods G. Low density flexible foams. The ICI Polyurethanes Book. John Willey and Sons; 1990. p. 55–84.
19. Woods G. Rigid polyurethane foams. The ICI Polyurethanes Book. John Willey and Sons; 1990. p. 127–74.
20. Purohit BK, Sistla VS. Crystallization of inorganic salt hydrates in polymeric foam for thermal energy storage application. J Energy Storage. 2017;12:196–201. https://doi.org/10.1016/j.est.2017.05.001.
21. Albert C, Cristian S. Design of latent heat storage systems using phase change materials (PCMs). In: Ltd E, editor. Advances in Thermal Energy Storage Systems. Woodhead; 2015. p. 285–305.
22. Döğüşcü DK, Altıntaş A, Sarı A, Alkan C. Polystyrene microcapsules with palmitic-capric acid eutectic mixture as building thermal energy storage materials. Energy Build. 2017;150:376–82. https://doi.org/10.1016/j.enbuild.2017.06.022.
23. Villasmil W, Fischer LJ, Worlitschek J. A review and evaluation of thermal insulation materials and methods for thermal energy storage systems. Renew Sustain Energy Rev. 2019;103:71–84. https://doi.org/10.1016/j.rser.2018.12.040.
24. Mert MS, Mert HH, Sert M. Microencapsulated oleic–capric acid/hexadecane mixture as phase change material for thermal energy storage. J Therm Anal Calorim. 2018;136(4):1551–61. https://doi.org/10.1007/s10973-018-7815-5.
25. Kong W, Lei Y, Jiang Y, Lei J. Preparation and thermal performance of polyurethane/PEG as novel form-stable phase change materials for thermal energy storage. J Therm Anal Calorim. 2017;130(2):1011–9. https://doi.org/10.1007/s10973-017-6467-1.
26. Qiu X, Lu L, Zhang Z, Tang G, Song G. Preparation, thermal property, and thermal stability of microencapsulated n-octadecane with poly(stearyl methacrylate) as shell. J Therm Anal Calorim. 2014;118(3):1441–9. https://doi.org/10.1007/s10973-014-4040-8.
27. Royon L, Karim L, Bontemps A. Thermal energy storage and release of a new component with PCM for integration in floors for thermal management of buildings. Energy Build. 2013;63:29–35. https://doi.org/10.1016/j.enbuild.2013.03.042.
28. Ling T-C, Poon C-S. Use of phase change materials for thermal energy storage in concrete: An overview. Constr Build Mater. 2013;46:55–62. https://doi.org/10.1016/j.conbuildmat.2013.04.031.
29. Refat AS, Farid M. Microencapsulation of phase change materials (PCMs) for thermal energy storage systems. In: Cabeza LF, editor. Advances in Thermal Energy Storage Systems. Woodhead Publisher; 2015. p. 247–84.
30. Kuznik F, Johannes K, David D. Integrating phase change materials (PCMs) in thermal energy storage systems for buildings. In: Cabeza LF, editor. Advances in Thermal Energy Storage Systems. Woodhead Publishing; 2015. p. 325–53.
31. Zhang H, Wang X. Fabrication and performances of microencapsulated phase change materials based on n-octadecane core and resorcinol-modified melamine–formaldehyde shell. Colloids Surf A. 2009;332(2–3):129–38. https://doi.org/10.1016/j.colsurfa.2008.09.013.
32. Wang X, Zhao T. Effects of parameters of the shell formation process on the performance of microencapsulated phase change materials based on melamine-formaldehyde. Text Res J. 2016;87(15):1848–59. https://doi.org/10.1177/0040517516659382.
33. Su J, Wang X, Dong H. Influence of temperature on the deformation behaviors of melamine–formaldehyde microcapsules containing phase change material. Mater Lett. 2012;84:158–61. https://doi.org/10.1016/j.matlet.2012.06.074.
34. Su J, Wang L, Ren L. Fabrication and thermal properties of micro-PCMs: Used melamine-formaldehyde resin as shell material. J Appl Polym Sci. 2006;101(3):1522–8. https://doi.org/10.1002/app.23151.
35. Kavitha K, Arumugam S. Performance of paraffin as PCM solar thermal energy storage. Int J Renew Energy Res. 2013;3:1–5.
36. Hasan MI, Basher HO, Shdhan AO. Experimental investigation of phase change materials for insulation of residential buildings. Sustain Cities Soc. 2018;36:42–58. https://doi.org/10.1016/j.scs.2017.10.009.
37. Han P, Qiu X, Lu L, Pan L. Fabrication and characterization of a new enhanced hybrid shell microPCM for thermal energy storage. Energy Convers Manage. 2016;126:673–85. https://doi.org/10.1016/j.enconman.2016.08.052.
38. Alinejad Z, Khakzad F, Rezaee S-A. Preparation of Melamine - Formaldehyde Microcapsules Containing Hexadecane as a Phase Change Material. Iran J Polym Sci Technol. 2013;26(1):33–44.
39. Younsi Z, Naji H. Numerical simulation and thermal performance of hybrid brick walls embedding a phase change material for passive building applications. J Therm Anal Calorim. 2019;140(3):965–78. https://doi.org/10.1007/s10973-019-08950-x.
40. Bai G, Fan Q, Song X-M. Preparation and characterization of pavement materials with phase-change temperature modulation. J Therm Anal Calorim. 2019;136(6):2327–31. https://doi.org/10.1007/s10973-018-7862-y.
41. Dorigato A, Fredi G, Pegoretti A. Application of the thermal energy storage concept to novel epoxy-short carbon fiber composites. J Appl Polym Sci. 2019. https://doi.org/10.1002/app.47434.
42. Fredi G, Dorigato A, Fambri L, Pegoretti A. Wax confinement with carbon nanotubes for phase changing epoxy blends. Polyme. 2017. https://doi.org/10.3390/polym9090405.
43. Fredi G, Dorigato A, Pegoretti A. Multifunctional glass fiber/polyamide composites with thermal energy storage/release capability. Express Polym Lett. 2018;12(4):349–64. https://doi.org/10.3144/expresspolymlett.2018.30.
44. Fredi G, Dorigato A, Pegoretti A. Novel reactive thermoplastic resin as a matrix for laminates containing phase change microcapsules. Polym Compos. 2019;40(9):3711–24. https://doi.org/10.1002/pc.25233.
45. Dorigato A, Canclini P, Unterberger SH, Pegoretti A. Phase changing nanocomposites for low temperature thermal energy storage and release. Express Polym Lett. 2017;11(9):738–52. https://doi.org/10.3144/expresspolymlett.2017.71.
46. Dorigato A, Ciampolillo MV, Cataldi A, Bersani M, Pegoretti A. Polyethylene wax/epdm blends as shape-stabilized phase change materials for thermal energy storage. Rubber Chem Technol. 2017;90(3):575–84. https://doi.org/10.5254/rct.82.83719.
47. Gama NV, Amaral C, Silva T, Vicente R, Coutinho JAP, Barros-Timmons A, et al. Thermal energy storage and mechanical performance of crude glycerol polyurethane composite foams containing phase change materials and expandable graphite. Materials. 2018. https://doi.org/10.3390/ma11101896.
48. Dorigato A, Rigotti D, Pegoretti A. Thermoplastic polyurethane blends with thermal energy storage/release capability. Front Mater. 2018;5:58. https://doi.org/10.3389/fmats.2018.00058.
49. Rigotti D, Dorigato A, Pegoretti A. 3D printable thermoplastic polyurethane blends with thermal energy storage/release capabilities. Mater Today Commun. 2018;15:228–35. https://doi.org/10.1016/j.mtcomm.2018.03.009.
50. Fredi G, Dorigato A, Unterberger S, Artuso N, Pegoretti A. Discontinuous carbon fiber/polyamide composites with microencapsulated paraffin for thermal energy storage. J Appl Polym Sci. 2019. https://doi.org/10.1002/app.47408.
51. Fredi G, Dorigato A, Pegoretti A. Dynamic-mechanical response of carbon fiber laminates with a reactive thermoplastic resin

containing phase change microcapsules. Mechanics of Time-Dependent Materials. In Press. doi:https://doi.org/10.1007/s11043-019-09427-y.
52. Fredi G, Dorigato A, Fambri L, Pegoretti A. Multifunctional epoxy/carbon fiber laminates for thermal energy storage and release. Compos Sci Technol. 2018;158:101–11. https://doi.org/10.1016/j.compscitech.2018.02.005.
53. Borreguero AM, Rodríguez JF, Valverde JL, Peijs T, Carmona M. Characterization of rigid polyurethane foams containing microencapsulted phase change materials: Microcapsules type effect. J Appl Polym Sci. 2013;128(1):582–90. https://doi.org/10.1002/app.38226.
54. Amaral C, Vicente R, Ferreira VM, Silva T. Polyurethane foams with microencapsulated phase change material: Comparative analysis of thermal conductivity characterization approaches. Energy Build. 2017;153:392–402. https://doi.org/10.1016/j.enbuild.2017.08.019.
55. Serrano A, Borreguero AM, Garrido I, Rodríguez JF, Carmona M. The role of microstructure on the mechanical properties of polyurethane foams containing thermoregulating microcapsules. Polym Test. 2017;60:274–82. https://doi.org/10.1016/j.polymertesting.2017.04.011.
56. You M, Zhang XX, Li W, Wang XC. Effects of MicroPCMs on the fabrication of MicroPCMs/polyurethane composite foams. Thermochim Acta. 2008;472(1–2):20–4. https://doi.org/10.1016/j.tca.2008.03.006.
57. You M, Zhang X, Wang J, Wang X. Polyurethane foam containing microencapsulated phase-change materials with styrene–divinybenzene co-polymer shells. J Mater Sci. 2009;44(12):3141–7. https://doi.org/10.1007/s10853-009-3418-7.
58. Yang C, Fischer L, Maranda S, Worlitschek J. Rigid polyurethane foams incorporated with phase change materials: A state-of-the-art review and future research pathways. Energy Build. 2015;87:25–36. https://doi.org/10.1016/j.enbuild.2014.10.075.
59. Serrano A, Borreguero AM, Garrido I, Rodríguez JF, Carmona M. Reducing heat loss through the building envelope by using polyurethane foams containing thermoregulating microcapsules. Appl Therm Eng. 2016;103:226–32. https://doi.org/10.1016/j.applthermaleng.2016.04.098.
60. Sarier N, Onder E. Thermal characteristics of polyurethane foams incorporated with phase change materials. Thermochim Acta. 2007;454(2):90–8. https://doi.org/10.1016/j.tca.2006.12.024.
61. Du X, Li J, Wang S, Wang H, Cheng X, Du Z. Fabrication and characterization of polyurethane foams containing phase change materials for thermal energy storage. Thermochim Acta. 2018;670:55–60. https://doi.org/10.1016/j.tca.2018.10.014.
62. Telma M, Nelson S, Isabel C-G, José JC, Pedro NS, Luísa D, editors. Thermophysical characterization of commercial para n-based pcms for low temperature thermal energy storage applications. Proc of the Seminar PCMs4Buildings—PCMs: Thermophysical characterization and buildings' applications; 2018; Coimbra: Department of Chemical Engineering-University of Coimbra.